



HAL
open science

Time-Dependent Elastic Tensor of Cellulose Nanocrystal Probed by Hydrostatic Pressure and Uniaxial Stretching

Guangjie Song, Christine Lancelon-Pin, Pan Chen, Jian Yu, Jun Zhang, Lei Su, Masahisa Wada, Tsunehisa Kimura, Yoshiharu Nishiyama

► **To cite this version:**

Guangjie Song, Christine Lancelon-Pin, Pan Chen, Jian Yu, Jun Zhang, et al.. Time-Dependent Elastic Tensor of Cellulose Nanocrystal Probed by Hydrostatic Pressure and Uniaxial Stretching. *Journal of Physical Chemistry Letters*, 2021, 12 (15), pp.3779-3785. 10.1021/acs.jpcllett.1c00576 . hal-03764690

HAL Id: hal-03764690

<https://hal.science/hal-03764690>

Submitted on 30 Aug 2022

HAL is a multi-disciplinary open access archive for the deposit and dissemination of scientific research documents, whether they are published or not. The documents may come from teaching and research institutions in France or abroad, or from public or private research centers.

L'archive ouverte pluridisciplinaire **HAL**, est destinée au dépôt et à la diffusion de documents scientifiques de niveau recherche, publiés ou non, émanant des établissements d'enseignement et de recherche français ou étrangers, des laboratoires publics ou privés.

Time-Dependent Elastic Tensor of Cellulose Nanocrystal Probed by Hydrostatic Pressure and Uniaxial Stretching

Guangjie Song,[†] Christine Lancelon-Pin,[‡] Pan Chen,[¶] Jian Yu,[†] Jun Zhang,^{*,†}
Lei Su,^{*,§} Masahisa Wada,^{||} Tsunehisa Kimura,^{||,⊥} and Yoshiharu Nishiyama^{*,‡}

[†]*Beijing National Laboratory for Molecular Sciences, CAS Key Laboratory of Engineering
Plastics, Institute of Chemistry, Chinese Academy of Sciences (CAS), Beijing 100190,
China*

[‡]*Univ. Grenoble Alpes, CNRS, CERMAV, 38000 Grenoble, France*

[¶]*Beijing Engineering Research Center of Cellulose and its Derivatives, School of Materials
Science and Engineering, Beijing Institute of Technology, 5 South Zhongguancun Street,
Haidian District, Beijing 100081, China*

[§]*CAS Key Laboratory of Photochemistry, Institute of Chemistry, Chinese Academy of
Sciences (CAS), Beijing 100190, China*

^{||}*Division of Forest and Biomaterials Science, Kyoto University, Sakyo-ku, Kyoto
606-8502, Japan*

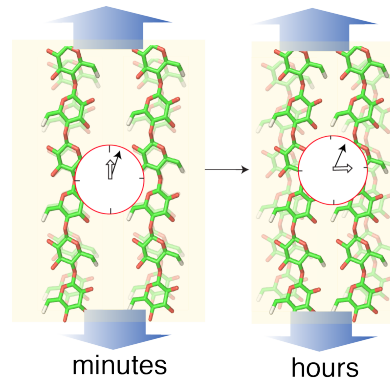
[⊥]*Current address: Fukui University of Technology, 3-6-1 Gakuen, Fukui 910-8505, Japan*

E-mail: jzhang@iccas.ac.cn; leisu2050@iccas.ac.cn; yoshi@cermav.cnrs.fr

Abstract

The elastic properties of crystals are fundamental for structural material. However, in the absence of macroscopic single crystals, the experimental determination of the elastic tensor is challenging because the measurement depends on the transmission of stress inside the material. To avoid arbitrary hypotheses about stress transfer, we combine hydrostatic pressure and uniaxial-stretching experiments to investigate the elastic properties of cellulose I_{β} . Three orthogonal compressibilities are 50.0, 6.6, and 1.71 TPa^{-1} . Combining Poisson's ratios from a uniaxial stretching experiment directly gives the Young's modulus along the chain direction (E_{33}). However, Poisson's ratio depends on the deformation rate leading to apparent modulus $E_{33} = 113 \text{ GPa}$ using a slow cycle (hours), and 161 GPa using a fast cycle (minutes). The lattice deformation along the chain is not time dependent, so the off-diagonal elements are time-dependent on the scale of minutes to hours.

Graphical TOC Entry



Cellulose exists in nature as slender crystalline microfibrils with nanometric lateral dimensions and form the main tensile-load-bearing components in plants, wood, and fiber products.¹ Thus, the intrinsic elastic properties of cellulose crystals are of fundamental interest.^{2,3} The most abundant cellulose allomorph is I_{β} ,⁴ which has a monoclinic unit cell (Fig. 1). In this case, the elastic tensor has 13 independent elements⁵ in the framework of continuum mechanics and is highly anisotropic because the bonding depends on direction. However, in the absence of macroscopic single crystals, the experimental determination of these tensor elements is challenging.

A straightforward experimental technique to probe the elastic properties of crystals is to stretch a bundle of well-aligned crystalline fibers, such as ramie fiber, while monitoring the lattice spacing along the chain direction. For ramie fibers, several studies give a reproducible crystal modulus of 127–138 GPa along the chain direction.^{6,7} The sharp diffraction peak allows the lattice strain to be determined to high precision. However, converting load to stress in the crystal is less straightforward because the cross section of natural fibers are irregular and may even contain voids. To overcome this difficulty, Sakurada and Nishino estimated the fiber cross sections from the weight-per-length of dry samples and then used the sample or crystal density to derive the effective cross section. In their work, the macroscopic modulus of the fiber was less in the wet state than in the dry state, whereas the lattice displacement as a function of load remained unchanged between the two states, so they assumed that stress was completely transmitted to the crystallites. Conversely, if one considers the natural fibers to have crystalline domains and amorphous phases not only when arranged in series, then estimating the crystalline modulus becomes more complicated.^{8,9}

Another experimental technique to probe the elastic properties of crystals consists of using an atomic force microscope to bend crystal samples,¹⁰ where the cross-sectional crystal shape is decisive and the force needed to bend the crystal to the same extent is proportional to the crystal height cubed. The phonon velocity obtained by x-ray inelastic scattering gives 220 ± 50 GPa along the c direction and 15 ± 1 GPa along the a^* direction.¹¹

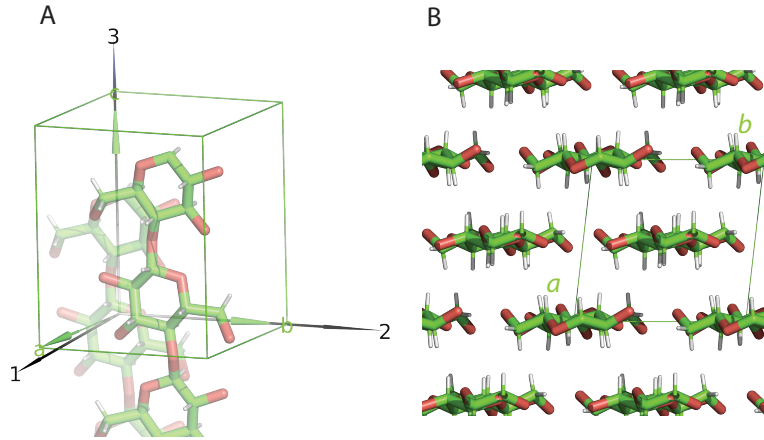


Figure 1: (A) Cellulose I_{β} unit cell and Cartesian bases used in this study. (B) Projection of crystal structure along fiber axis.

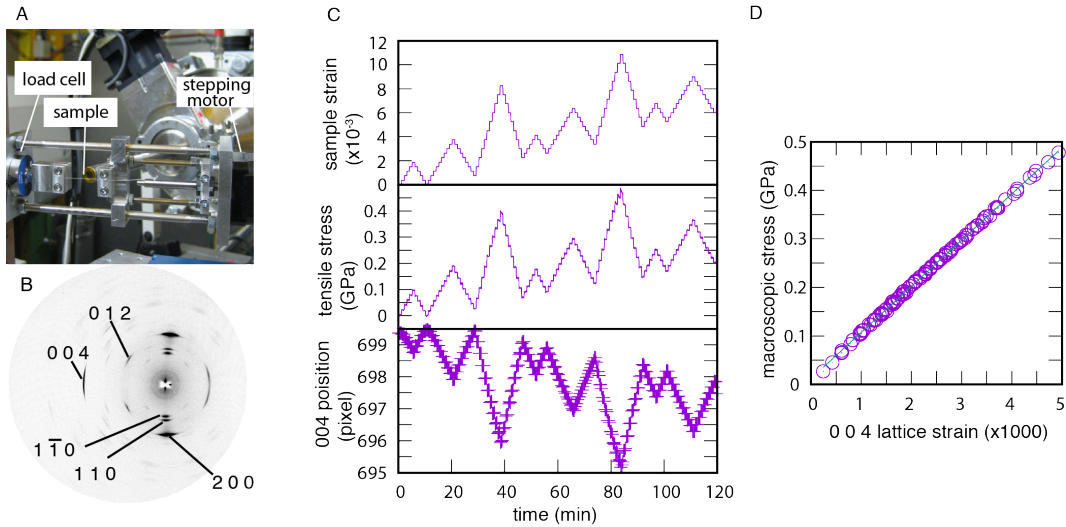


Figure 2: Uniaxial-stretching experiment to measure lattice strain. (A) Sample-mounting setup on beamline A2 at DESY. (B) Typical x-ray diffraction pattern with indices given for major diffraction spots. (C) (top) Results of typical cyclic-loading experiment with step-wise sample strain imposed, (middle) macroscopic tensile stress, and (0 0 4) peak position, all as functions of time. (D) Macroscopic stress versus (0 0 4) lattice strain of cellulose for cellulose-PVA composite fiber with 72% cellulose.

The elastic tensor can also be predicted theoretically to different levels of precision. To calculate the elastic tensor of cellulose, density-functional theory (DFT) with dispersion correction depends less on *ad hoc* parameters than on modeling based on molecular force fields. Dri *et al.* used simple stress derivatives to estimate the Young's modulus along the cellulose chain axis at 206 GPa,¹² and other estimates give 202 GPa at 0 K and 196 GPa

at 300 K¹³ upon accounting for thermal vibrations. These values fall within the range of estimates based on x-ray inelastic scattering measurements but are substantially greater than estimates based on tensile measurements. In addition, no experimental validation exists for other tensor elements.

Tunicin is cellulose from the mantle of sea animals, and serves as typical model cellulose because it has the same crystal structure (i.e., I_β allomorph) as most native cellulose but with a much larger crystallite size (on the order of 10–20 nm), so it produces well-resolved diffraction peaks.⁴ In this work, we combine hydrostatic pressure and uniaxial-stretching experiments to obtain the Young’s modulus of cellulose crystals.

In the generalized form of Hooke’s law, the elastic tensor relates the strain tensor ϵ to the stress σ as

$$\epsilon = S\sigma, \tag{1}$$

where S is the compliance matrix.⁵ For a monoclinic continuum system,

$$S = \begin{pmatrix} s_{11} & s_{12} & s_{13} & 0 & 0 & s_{16} \\ s_{21} & s_{22} & s_{23} & 0 & 0 & s_{26} \\ s_{31} & s_{32} & s_{33} & 0 & 0 & s_{36} \\ 0 & 0 & 0 & s_{44} & s_{45} & 0 \\ 0 & 0 & 0 & s_{54} & s_{55} & 0 \\ s_{61} & s_{62} & s_{63} & 0 & 0 & s_{66} \end{pmatrix}. \tag{2}$$

A hydrostatic experiment allows us to determine the relation

$$\begin{pmatrix} \epsilon_1 \\ \epsilon_2 \\ \epsilon_3 \\ \epsilon_6 \end{pmatrix} = \begin{pmatrix} s_{11} & s_{12} & s_{13} \\ s_{21} & s_{22} & s_{23} \\ s_{31} & s_{32} & s_{33} \\ s_{61} & s_{62} & s_{63} \end{pmatrix} \begin{pmatrix} \sigma \\ \sigma \\ \sigma \end{pmatrix}, \tag{3}$$

which is related to the compressibility X_i along direction i as

$$X_i = \sum_j s_{ij}. \quad (4)$$

In addition, based on uniaxial stretching of a composite fiber and assuming that the fraction of apparent stress a transits through the crystal, we obtain

$$\begin{pmatrix} \epsilon_1 \\ \epsilon_2 \\ \epsilon_3 \\ \epsilon_6 \end{pmatrix} = a\sigma \begin{pmatrix} s_{13} \\ s_{23} \\ s_{33} \\ s_{36} \end{pmatrix}, \quad (5)$$

from which Poisson's ratios

$$\nu_{ij} = -s_{ij}/s_{ii} \quad (6)$$

can be obtained. Even if a is unknown, if the tensor is symmetric (i.e., $s_{ij} = s_{ji}$), we should be able to combine two experimental observations to obtain Young's modulus along the chain axis as

$$E_{33} = \frac{1}{s_{33}} = \frac{1 - \nu_{31} - \nu_{32}}{X_3}. \quad (7)$$

As we see later, this estimation of E_{33} is highly dependent on Poisson's ratios, but we can measure them quite accurately. Equations (3) and (5) gives seven independent observations that can be directly compared with theoretical predictions.

Figure 2 presents a typical uniaxial-stretching experiment involving a composite fiber of highly oriented (standard deviation of 4° , Hermans orientation parameter¹⁴ of 0.98) tunicin embedded in an amorphous poly(vinyl alcohol) matrix, with the fiber axis horizontal and tilted with respect to the plane normal to the incident beam to bring the 0 0 4 reflection into the Bragg condition. This gives the asymmetric fiber pattern shown in Fig. 2B. Figure 2C gives an overview of a measurement in which the macroscopic sample strain reaches about

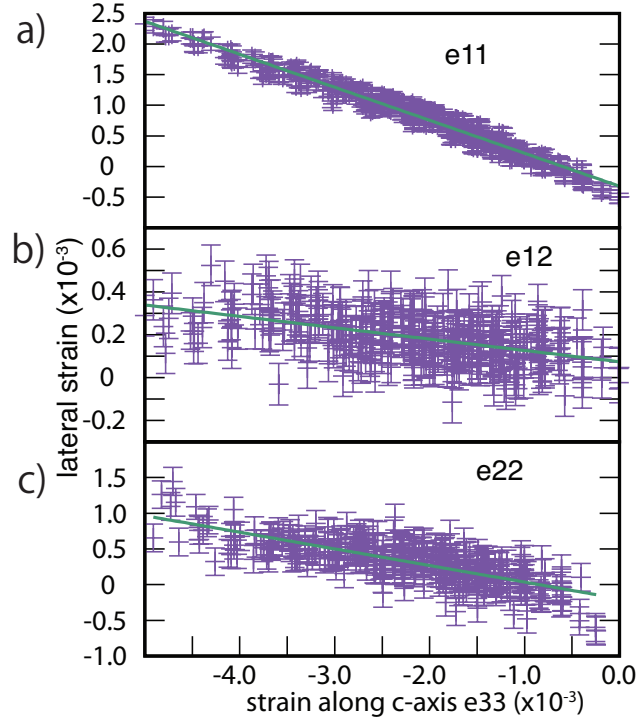


Figure 3: Lateral Lagrange strains a) e_{11} , b) e_{12} and c) e_{22} as a function of 0 0 4 lattice strain in the uniaxial-stretching experiment. Solid lines are weighted least-squares fit to the data.

1%, the macroscopic tensile stress on the whole fiber reaches about 0.5 GPa based on the load cell read-out, and the 0 0 4 reflection shifts by up to 5 pixels as a function of time. The sample strain was maintained for 1 minute, during which three diffraction patterns were recorded. The macroscopic strain was applied cyclically at different amplitudes to verify that the process is reversible. At higher strain, the tensile stress tends to relax, which is probably due to the viscoelasticity of the PVA matrix, but the stress remains proportional to the crystal strain over the whole experiment (2D).

The weight fraction of cellulose in our sample was 72%, corresponding to a volume fraction (ϕ) of 65%. If we assume that 100% of the load is transmitted through the cellulose, then Young's modulus E_{33} along the chain direction would be 153 ± 3 GPa, which is the higher bound. Since the aspect ratio of tunicin is above 50,¹⁵ one could consider the composite as

parallel system (uniform strain), in which case the stress-strain (σ - ϵ) relation becomes

$$\sigma = [\phi E_{33} + (1 - \phi) E_{\text{PVA}}] \epsilon \quad (8)$$

attenuating the stress transferred through crystal by $(1 - \phi)/\phi E_{\text{PVA}}$ so the Young's modulus of cellulose along chain would be

$$E_{33} = 153 - 0.54 E_{\text{PVA}} \text{ [GPa]}, \quad (9)$$

where E_{PVA} is the effective modulus of PVA matrix. In reality this is an underestimation since the macroscopic strain is larger than the lattice strain. Although individual crystals have high aspect ratio, they can form domains of lower aspect ratio. A typical modulus of neat PVA samples prepared in the same condition is in range of 10 – 15 GPa, so the contribution of the second term would be below 10 GPa.

Figure 3 shows the Lagrangian strains in the **1-2** plane as a function of strain along **3**, with weighted least-squares fits shown as solid lines. The strains are calculated from the shift in the diffraction peak, as detailed in Sec. 1 of the Supplemental Information (SI). The slopes correspond to the negative of the Poisson ratios, $-\nu_{3i}$. Figure 1 shows the reference frame used (i.e., **1** is parallel to the a^* axis and **3** is parallel to the c axis).

Figure 4A shows the x-ray diffraction data acquired with the sample under hydrostatic pressure in a diamond anvil cell, and Fig. 4B shows the resulting diffraction profiles of tunicin as a function of pressure. The 2 0 0 diffraction intensity decreases by about 15% at 2.7 GPa with respect to ambient conditions, whereas the other diffraction peaks labeled in the figure remain essentially constant (within a few percent). The 0 0 4 d spacing varies linearly with pressure below 3 GPa, whereas the d spacings of other equatorial reflections vary parabolically with pressure (Fig. 4C).

The errors estimated for ϵ_{33} and ϵ_{11} are small because of the sharpness of the 0 0 4 and 2 0 0 diffraction peaks. However, ϵ_{22} and ϵ_{12} fluctuate slightly due to the low intensity and

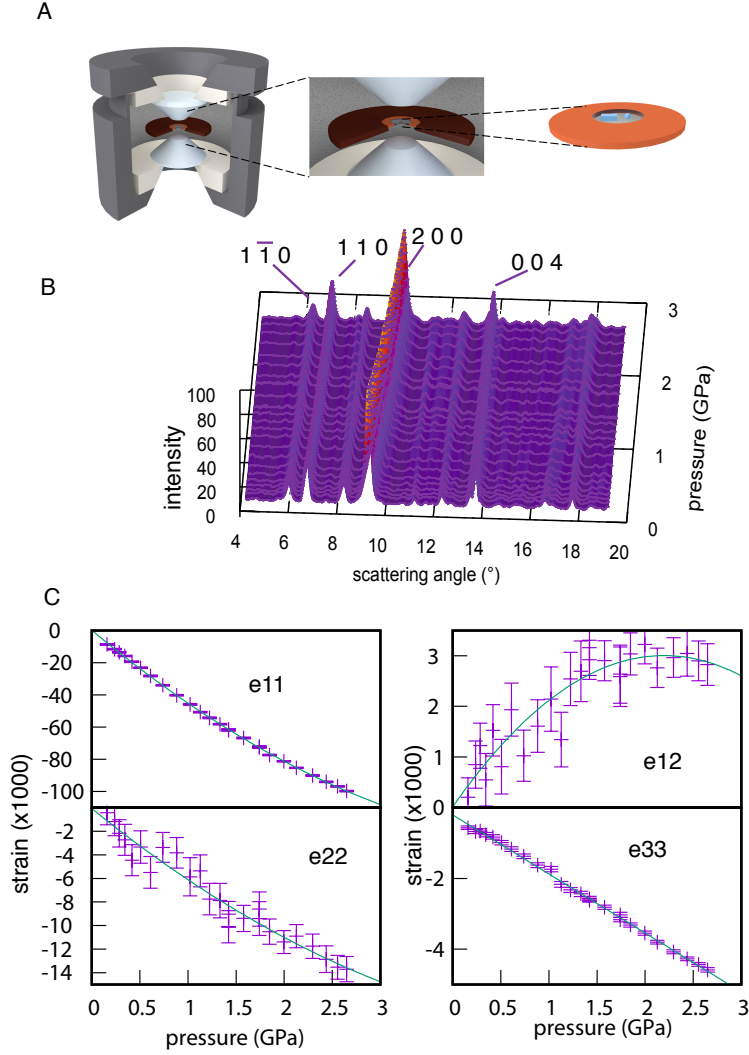


Figure 4: X-ray diffraction under hydrostatic pressure. (A) Schematic illustration of diamond anvil cell with cellulose sample mounted and ruby as calibrant using fluorescence. (B) Diffraction profile as a function of pressure after subtraction of background using the Sonneveld algorithm.¹⁶ (C) Components of Lagrange strain deduced from peak positions in panel (B) as a function of pressure.

high background in the $1\bar{1}0$ reflection. Still, the statistics are sufficient to determine the strain tensor as a function of hydrostatic pressure.

Table 1 summarizes the measured compressibility, Poisson's ratio, and off-diagonal tensor elements obtained from the curve fit in Figs. 4 and 3 as well as from theoretical calculations and from the literature. Although the experimentally determined hydrostatic pressure on the cotton is consistent with our result for X_1 , the compressibility in other directions is not

available, and the deformation data contain uninterpreted outliers, especially with respect to the chain direction (direction **3**). Given the small compressibility in this direction, a precise measurement would require a stable experimental setup. We improved the precision of X_1 and X_3 by over an order of magnitude and determined X_2 and X_6 with 15% accuracy.

When compared with the compressibility obtained from elastic tensors deduced by DFT, the present experimental results for X_1 and X_2 lie between the values obtained with and without the inclusion of thermal vibrations. However, the measured compressibility along the chain direction X_3 is much less than that obtained from the DFT tensor. We also used DFT to calculate the elastic properties by (1) combining deformations and (2) imposing hydrostatic stress equivalent to that imposed by a hydrostatic-pressure experiment, and the resulting compressibilities are closer to the experimental values (including X_3). Conversely, all DFT calculations are consistent with the experimentally determined elastic modulus E_{33} to be in the range of 195–207 GPa.

Although uniaxial-stretching experiments with the strain monitored by x-ray diffraction are not new,⁶ efforts to monitor Poisson’s ratio are relatively recent.¹⁹ Poisson’s ratio ν_{31} from higher plant cellulose such as ramie fibers has been reported by several groups. The results for ramie fibers are relatively scattered from 0.4 to 0.6 and, for kraft cooked wood pulp, an apparent negative Poisson ratio was reported. This apparent result, which is not an intrinsic property of the crystal, was attributed to the stress component being perpendicular to the hydrogen-bonded sheets or to the shear stress²¹ occurring inside the fiber during the tensile tests.

Due to the highly anisotropic nature of the mechanical properties and the slight tilt of the crystals with respect to the fiber axis, complex internal stress is likely to affect the apparent Poisson ratio. The slight differences in results from different samples may be due in part to partial structural modification that, while being to a much smaller extent than with kraft cooking, could still induce tensile stress orthogonal to the chain direction. Another problem with some of the published experimental report is that the incident x-ray beam was normal

to the stretching direction, so the crystals that were probed for axial deformation along the chain direction were inclined by θ (i.e., half the scattering angle) with respect to the stretching direction. This complicates the data interpretation in Ref.²⁰ and may have led to an underestimation of the chain stretching and a concomitant overestimation of Poisson's ratio.

In the current experiment, only crystals that are parallel to the stretching direction contribute to the 0 0 4 diffraction intensity. Poisson's ratios obtained from elastic tensors calculated by DFT or force-field are in general lower than the experimentally determined ratios. Upon considering thermal vibrations, dispersion-corrected DFT produces an even lower Poisson ratio. In other words, the axial strains are uncoupled, which is probably due to reduced intermolecular interactions resulting from increased intermolecular distances as the cell parameter a increases to 7.896 Å at 300 K rather than 7.56 Å, as per the simple energy minimization by the same authors.¹² Despite the significant discrepancy between theoretical predictions and the present measurements, our experimental Poisson-ratio estimates are reliable because we find no mechanisms in our current setup to produce a higher Poisson ratio.

Using Eq. (7) and the present experimental results, Young's modulus E_{33} along the chain direction is 113 GPa, which is much lower than other published estimates. Based on our stress measurement, the effective modulus of the amorphous PVA in the sample must be as high as 74 GPa, which is impossible. Although the experimental compressibility X_3 is lower than that determined by numerical simulation (i.e., the structure deforms less under pressure), Young's modulus E_{33} is less than that calculated by DFT. E_{33} of 113 GPa is also less than estimates from lattice strain measured on pure oriented fiber such as ramie, which are usually taken as benchmarks. Given the large crystallite sizes and slightly denser packing, we expected a larger E_{33} .

The small estimated Young's modulus along the chain is related to the large Poisson ratios. The estimated Young's modulus is linearly related to the sum of the Poisson ratios

ν_{31} and ν_{32} , and a 10% change in the sum modifies the estimated modulus by 58 GPa. For example, if Poisson ratio $\nu_{31} = 0.297$, as measured by Nakamura et al.¹⁹ on ramie fibers, the estimated Young’s modulus would increase to 277 GPa according to Eq. (7).

The stress in pure cellulose samples, even with high uniaxial orientation, can be complex due to the small tilt of the crystal axis with respect to the fiber direction. In this case, a non-negligible stress component develops perpendicular to the chain direction and constrains the deformation along the c axis, or, in the extreme case, produces a negative Poisson ratio.²¹ The extent of this effect depends on the fine structure of the fiber and the moisture content, resulting in a high variability in the Poisson ratio of different samples.²⁰ In this case, the crystal modulus measured from 0 0 4 displacement can appear larger and the Poisson ratio can be suppressed.

Note, however, that the simple linear elasticity analysis presented herein may overlook some factors, such as an asymmetric elastic tensor or a time dependence.

Equation (7) is based on the idea that the elastic tensor is symmetric. The uniaxial-stretching experiment measures s_{i3}/s_{33} , whereas the contribution to the compressibility X_3 is s_{3i} . One explanation for the small Young’s modulus calculated from the compressibility and Poisson’s ratio is that the elastic tensor of cellulose is not symmetric but $\sum s_{3i} < \sum s_{i3}$. Note that the orthotropic elastic tensor of wood²² is asymmetric on a macroscopic scale, although the mechanism is not understood.

To check whether the elastic tensor is asymmetric, we derive the elastic tensor without the symmetry constraint by using the stress given by the DFT deformation simulation. This leads to a difference of about 20% between s_{31} and s_{13} (Table 1), which suggests that, at the molecular level, cellulose cannot be considered as a continuum and thus can depart from the continuum mechanics description. However, the calculated tendency of the off-diagonal tensor elements to be asymmetric does not explain the discrepancy in E_{33} directly estimated from uniaxial stretching and estimated from a combination of compressibility and Poisson’s ratios, since $|s_{13}| + |s_{23}| < |s_{31}| + |s_{32}|$.

Is strain rate influencing the result? Figure 3 plots all the experimental strain relations together. In addition, we calculated the Poisson ratios from each loading and unloading segment, which each took about 10 minutes. This leads to average Poisson’s ratios of $\nu_{31} = 0.524 \pm 0.005$ and $\nu_{32} = 0.20 \pm 0.01$, which are significantly lower than those obtained by fitting to the data and lead to $E_{33} = 161 \pm 6$ GPa, consistent with the direct estimate from uniaxial stretching, and estimates from different methods in the literature.^{10,23}

The hydrostatic pressure experiment took about 2 h to reach 1 GPa, which is comparable to the duration of the uniaxial stretching experiment. However, the strain rate was 0.05 and 0.02 h⁻¹ along directions **1** and **2**, respectively, for the hydrostatic pressure experiment, which is about an order of magnitude greater, overall, than in the stretching experiment. In the stretching experiment, the strain rates during the 10 minute loading and unloading segments approach that of the hydrostatic experiment.

These results paint a picture of a time-dependent elastic tensor where the off-diagonal elements depend on the strain rate on a time scale of minutes to hours. Under slow deformation, coupling between normal deformations parallel and perpendicular to the chain direction would increase, leading to a low compressibility X_{33} and a high Poisson ratio. The DFT-calculated tensor corresponds to a fast deformation, where the coupling between the chain direction and the hydrogen-bonded direction is especially weak. The small deformation along the hydrogen-bonded direction in the DFT simulation may also result from a periodic constraint imposed in the simulation. Although loss of periodicity to fit a structure into a smaller space under pressure is common and is seen, for example, in ice crystals,²⁴ it is not possible in periodic DFT calculations based on a small cell. The response along the chain direction thus remains relatively constant in time, as can be seen from Fig. 2D, but the experimental estimates of Young’s modulus E_{33} may be smaller than that calculated by DFT partially because of a time dependence on a shorter time scale. This also corroborates the high modulus estimated based on inelastic x-ray scattering, which probes the fast response of the material, although the error is too large to be conclusive. We also measured

compressibility at different compression rates, which suggests a smaller compressibility at a higher compression rate (Table S1), but better data quality is required to confirm this result.

Experimental

Cellulose nanocrystals typically 10–20 nm wide and microns long were prepared from the mantle of sea animal tunicate. The mantle material was treated successively with 5% NaOH and a an equal-volume mixture of 0.3% NaClO₂ in 0.1 M acetate buffer (pH = 4.5). The material was then cut into pieces and disintegrated in a double-cylinder-type homogenizer (Physoctron, Microtec Nichion, Co., Tokyo) and treated with 50% H₂SO₄ at 70 °C for 8 h under strong stirring. A non-flocculating, flow-birefringent aqueous suspension of tunicate cellulose whiskers were obtained after thorough washing by centrifugation and dialysis against deionized water.

Uniaxially oriented samples embedded in polyvinyl alcohol (PVA: \approx 100 kDa, 99% saponified) matrix were prepared as previously reported.²⁵ Briefly, the \approx 4%-concentrated suspension of cellulose whiskers were mixed with 4% aqueous PVA solution. A drop of saturated borax solution was added to make a viscoelastic physical gel from which a fiber was slowly spun with the aid of tweezers. The gel was stretched and dried with a suspended weight to obtain uniaxial orientation. Finally, the borax was washed out with methanol and the sample was further dried in an oven at 80 °C.

For uniaxial measurement, a tensile tester was assembled using a 250 μ m stepper-motor actuator, a load sensor from Loadstar Sensors (Fremont, USA), and guide shafts, as shown in Fig. 3A. The apparatus was installed horizontally at beamline A2 of HASYLAB, Hamburg. The tester was positioned so that the sample was oriented at about 17° with respect to the plane normal to the incident beam, bringing the 0 0 4 reflection along the stretching direction into the Bragg condition. A MAR165 detector served to record the x-ray diffraction pattern, and the peak positions were fit to two-dimensional pseudo-Voigt functions to extract the

peak positions and convert the data to Lagrangian strain, as detailed in the SI.

X-ray diffraction experiments under hydrostatic pressure at room temperature were done at High-Pressure Station 4W2 of the Beijing Synchrotron Radiation Facility.²⁶ A 0.6199 Å (20 keV) beam with a $36 \times 14 \mu\text{m}^2$ spot served as light source, and a Pilatus3 2M area detector recorded the diffraction pattern. The sample was 30 cm from the detector, and the beam center and detector tilt with respect to the incident beam were calibrated by using CeO_2 powder. Screw-driven diamond anvil cells with culet diameters of 800 μm applied the pressure. The sample was contained in a stainless steel gasket pre-indented to a thickness of about 100 μm and with a hand-drilled 400- μm -diameter hole. Small ruby spheres were added to determine the pressure *in situ* by using the fluorescence method implemented with a 532 nm laser.²⁷ The pressure was transmitted by a 4 : 1 mixture of methanol and ethanol.

For each pressure point, the data were acquired by (1) manually turning the screws, (2) measuring the ruby fluorescence, (3) allowing the pressure to equilibrate for 5 to 10 minutes, (4) acquiring the diffraction pattern for 450 s, and (5) again measuring the ruby fluorescence. The pressure before and after data acquisition varied by less than 50 MPa. The experimental details are available in Sec. 2 of the SI.

Computational Methods

The elements of the symmetric elastic tensor were estimated by using the energy-strain approach.²⁸ Thirteen deformation modes were generated to deduce the 13 tensor elements of the monoclinic unit cell of cellulose I_β .⁴ The geometry of each deformed structure was optimized by using a periodic DFT calculation implemented in the Quantum Espresso package (version 6.6)²⁹ using the generalized gradient approximation (GGA), the Perdew, Burke, Ernzerhof functional, and the pairwise DFT-D2 correction for long-range van der Waals dispersion. The results were fit to obtain the second derivative of energy as a function of strain.

To calculate the 36 elements of the asymmetric tensor, we used the stress tensors for all deformations to determine the asymmetric tensor by linear least-squares fitting.

Energy optimization in DFT was also done under hydrostatic pressures ranging from 0 to 3 GPa in steps of 0.3 GPa. The isotropic compressibility was estimated directly from the optimized unit-cell parameters as a function of pressure.

The details of the simulations and a summary the results are available in Sec. 4 of the SI.

Acknowledgement

We thank Pierre Sailer for making the portable stretching device for the x-ray-monitored tensile tests. Part of the work was funded by ANR. We thank the staffs from the 4W2 beamline at the Beijing Synchrotron Radiation Facility (BSRF) and the 15U1 beamline at the Shanghai Synchrotron Radiation Facility (SSRF). The work was supported by the French National Research Agency (ANR-07-JCJC-0021), the National Key Research and Development Program of China (2017YFA0403103), and the National Natural Science Foundation of China (Grants No. 21704107 and No. 51425307). P.C. thanks the Beijing Natural Science Foundation (2204096) and the Beijing Institute of Technology Research Fund for Young Scholars.

Supporting Information Available

Details of data processing and numerical simulations are presented in supporting information.

References

- (1) Nishiyama, Y. Structure and Properties of Cellulose Microfibril. *J. Wood Sci.* **2009**, *55*, 241–249.

- (2) Eichhorn, S. J. Stiff as a Board: Perspectives on the Crystalline Modulus of Cellulose. *ACS Macro Letters* **2012**, *1*, 1237 – 1239.
- (3) Molnár, G.; Rodneyb, D.; Martoä, F.; Dumont, P. J. J.; Nishiyama, Y.; Mazeau, K.; Orgéas, L. Cellulose Crystals Plastify by Localized Shear. *Proceedings of the National Academy of Science* **2018**, *115*, 7260 –7265.
- (4) Nishiyama, Y.; Langan, P.; Chanzy, H. Crystal Structure and Hydrogen-Bonding System in Cellulose I β from Synchrotron X-ray and Neutron Fiber Diffraction. *J. Am. Chem. Soc.* **2002**, *124*, 9074–9082.
- (5) Nye, J. F. *Physical Properties of Crystals : Their Representation by Tensors and Matrices*; Clarendon Press: Oxford, 1985.
- (6) Sakurada, I.; Ito, T.; Nakamae, K. Elastic Moduli of the Crystal Lattices of Polymers. *J. Polym. Sci. C* **1966**, *15*, 75–91.
- (7) Nishino, T.; Takano, K.; Nakamae, K. Elastic Modulus of the Crystalline Regions of Cellulose Polymorphs. *J. Polym. Sci., Part B: Polym. Phys.* **1995**, *33*, 1647–1651.
- (8) Matsuo, M.; Sawatari, C.; Iwai, Y.; F, O. Effect of Orientation Distribution and Crystallinity on the Measurement of X-ray Diffraction of the Crystal Lattice Moduli of Cellulose I and II. *Macromolecules* **1990**, *23*, 3266–3275.
- (9) Ishikawa, A.; Okano, T.; Sugiyama, J. Fine Structure and Tensile Properties of Ramie Fibres in the Crystalline Form of Cellulose I, II, III_I and IV_{II}. *Polymer* **1997**, *38*, 463–468.
- (10) Iwamoto, S.; Kai, W.; Isogai, A.; Iwata, T. Elastic Modulus of Single Cellulose Microfibrils from Tunicate Measured by Atomic Force Microscopy. *Biomacromolecules* **2009**, *10*, 2571 – 2576.

- (11) Diddens, I.; Murphy, B.; Krisch, M.; Müller, M. Anisotropic Elastic Properties of Cellulose Measured using Inelastic X-ray Scattering. *Macromolecules* **2008**, *41*, 9755–9759.
- (12) Dri, F. L.; Hector, L. G., Jr.; Moon, R. J.; Zavattieri, P. D. Anisotropy of the Elastic Properties of Crystalline Cellulose I β from First Principles Density Functional Theory with Van der Waals Interactions. *Cellulose* **2013**, *20*, 2703–2718.
- (13) Dri, F. L.; Shang, S.; Hector, L. G., Jr.; Saxe, P.; Liu, Z.-K.; Moon, R. J.; Zavattieri, P. D. Anisotropy and Temperature Dependence of Structural, Thermodynamic and Elastic Properties of Crystalline Cellulose I β : a First-principles Investigation. *Modelling Simul. Mater. Sci. Eng.* **2014**, *22*, 085012.
- (14) Hermans, J. J.; Hermans, P. H.; Vermaas, D.; Weidinger, A. Quantitative evaluation of orientation in cellulose fibres from the X-ray fibre diagram. *Recueil des Travaux Chimiques des Pays-Bas* **1946**, *65*, 427–447.
- (15) Elazzouzi-Hafraoui, S.; Nishiyama, Y.; Putaux, J.-L.; Heux, L.; Dubreuil, F.; Rochas, C. The Shape and Size Distribution of Crystalline Nanoparticles Prepared by Acid Hydrolysis of Native Cellulose. *Biomacromolecules* **2008**, *9*, 57–65, PMID: 18052127.
- (16) Sonneveld, E. J.; Visser, J. W. Automatic collection of powder data from photographs. *Journal of Applied Crystallography* **1975**, *8*, 1–7.
- (17) Eichhorn, S. J.; Davies, G. R. Modelling the Crystalline Deformation of Native and Regenerated Cellulose. *Cellulose* **2006**, *13*, 291–307.
- (18) Cabrera, R. Q.; Meersman, F.; McMillan, P. F.; Dmitriev, V. Nanomechanical and Structural Properties of Native Cellulose under Compressive Stress. *Biomacromolecules* **2011**, *12*, 2178–2183.
- (19) Nakamura, K.; Wada, M.; Kuga, S.; Okano, T. Poisson's Ratio of Cellulose I β and Cellulose II. *J. Polym. Sci., Part B: Polym. Phys.* **2004**, *42*, 1206–1211.

- (20) Kölln, K. Morphologie und mechanische Eigenschaften von Zellulosefasern : Untersuchungen mit Röntgen- und Neutronenstreuung. Ph.D. thesis, Christian Albrechts Universität zur Kiel, 2004.
- (21) Peura, M.; Grotkopp, I.; Lemke, H.; Vikkula, A.; Laine, J.; Müller, M.; Serimaa, R. Negative Poisson Ratio of Crystalline Cellulose in Kraft Cooked Norway Spruce. *Biomacromolecules* **2006**, *7*, 1521–1528.
- (22) Hering, S.; Keunecke, D.; Niemz, P. Moisture Dependent Orthotropic Elasticity of Beech Wood. *Wood Science and Technology* **2012**, *46*, 927 – 938.
- (23) Šturcová, A.; Davies, G. R.; Eichhorn, S. J. Elastic Modulus and Stress-Transfer Properties of Tunicate Cellulose Whiskers. *Biomacromolecules* **2005**, *6*, 1055–1061, PMID: 15762678.
- (24) Mishima, O.; Calvert, L. D.; Whalley, E. 'Melting ice' I at 77K and 10 kbar: a New Method of Making Amorphous Solids. *Nature* **1984**, *310*, 393–395.
- (25) Nishiyama, Y.; Johnson, G. P.; French, A. D.; Forsyth, V. T.; Langan, P. Neutron Crystallography, Molecular Dynamics, and Quantum Mechanics Studies of the Nature of Hydrogen Bonding in Cellulose I_β. *Biomacromolecules* **2008**, *9*, 3133–3140.
- (26) Li, X.; Li, H.; Li, P.; Li, R.; Liu, J.; Li, Y.; Cui, W. A High-Pressure Single-Crystal-Diffraction Experimental System at 4W2 Beamline of BSRF. *Journal of Synchrotron Radiation* **2017**, *24*, 699–706.
- (27) Mao, H. K.; Bell, P. M.; Shaner, J. W.; Steinberg, D. J. Specific Volume Measurements of Cu, Mo, Pd, and Ag and Calibration of the Tuby R1 Fluorescence Pressure Gauge from 0.06 to 1 Mbar. *Journal of Applied Physics* **1978**, *49*, 3276–3283.
- (28) Golesorkhtabar, R.; Pavone, P.; Spitaler, J.; Puschnig, P.; Draxl, C. ElaStic: A Tool for

Calculating Second-Order Elastic Constants from First Principles. *Computer Physics Communications* **2013**, *184*, 1861–1873.

- (29) Giannozzi, P.; Andreussi, O.; Brumme, T.; Bunau, O.; Nardelli, M. B.; Calandra, M.; Car, R.; Cavazzoni, C.; Ceresoli, D.; Cococcioni, M. et al. Advanced Capabilities for Materials Modelling with Quantum ESPRESSO. *J. Phys.: Condens. Matter* **2017**, *29*, 465901.

Table 1: Elastic properties of cellulose I_β determined experimentally and theoretically.

	Units	Present study			Literature				
		X-ray diffraction	DFT (strain) ^a	DFT (stress) ^b	X-ray diffraction	MM ¹⁷ ^c	DFT ¹² ^c (300K)	DFT ^{13c}	
X_1	TPa ⁻¹	49.6 ± 0.4	61 ± 3	52.4 ± 0.6	50.5 ± 7.3^{18}	41.7	43.7 ± 0.7	61.4	
X_2		6.5 ± 1	5.0 ± 0.1	5.0 ± 0.2		10.6	4.3 ± 0.2	8.3	
X_3		1.71 ± 0.02	1.72 ± 0.02	1.64 ± 0.04	2.8 ± 0.4^{18}	3.7	2.16 ± 0.06	3.89	
X_6		-2.6 ± 0.4	8 ± 1	10 ± 2		10.7	-3.6 ± 3	8.6	
X'_1	TPa ⁻²	4.5 ± 0.2	10 ± 1	0		NA	NA	NA	
X'_2		0.5 ± 0.3	0.17 ± 0.02	0		NA	NA	NA	
X'_3		$\times 10^3$	0	0		NA	NA	NA	
X'_6		-0.6 ± 0.1	-1.7 ± 0.4	0		NA	NA	NA	
ν_{31}	TPa ⁻¹	0.577 ± 0.006	0.44 ± 0.02	0.52 ± 0.01	$0.32-0.64^{19,20}$	0.26	0.49 ± 0.01	0.21	
$-s_{13}$		3.7^d	5.1^e	2.2 ± 0.1		2.64 ± 0.04	1.8	2.60 ± 0.06	1.1
$-s_{31}$		NA	2.9 ± 0.1	2.90 ± 0.04					
ν_{32}	TPa ⁻¹	0.23 ± 0.01	-	0.059 ± 0.003		0.19	0.06 ± 0.002	0.03	
$-s_{23}$		$1.5 - 2.0$	-	0.59 ± 0.02		1.3	0.27 ± 0.01	0.15	
$-s_{32}$		NA	-	0.46 ± 0.01					
ν_{36}		0.057 ± 0.005	NA	0.55 ± 0.02		0.27	-0.37 ± 0.02	0.19	
E_{33}	GPa	153 ± 3^f 113 ± 6^g	202 ± 0.8	200.0 ± 0.1	135	146	206.5 ± 0.2	195	

^a By applying deformation. ^b By applying pressure. ^c After rotation of the tensor to match the frame (Sec. 3 of the SI). ^d Assuming $E_{33} = 153$ GPa. ^e Assuming $E_{33} = 113$ GPa. ^f From uniaxial stretching. ^g From compressibility and Poisson's ratios